Segmentation of Ultrasound Image Data by Two Dimensional Autoregressive Modelling

Phillip Abbott and Michael Braun

[1] Co-operative Research Centre for Cardiac Technology
Royal North Shore Hospital, St. Leonards, NSW, Australia
[2] Department of Applied Physics, University of Technology, Sydney
P.O.Box 123, Broadway 2007, NSW, Australia.
E-mail: phil@ihf.uts.edu.au

Abstract. In this paper we treat ultrasound image data as a two dimensional autoregressive (AR) signal. The image is modelled as consisting of distinct regions each described by one of a small number of AR models. Segmentation is performed by maximising the image likelihood function, which takes on a convenient form due to the AR model. Image data is presented to the algorithm in complex amplitude form. Results from application of this method to a cardiac phantom data set are presented.

1 Introduction

Ultrasound is a convenient, relatively inexpensive imaging modality. Its portability and real-time capability make it particularly suitable to diagnosis of cardiac dysfunction. Medical ultrasound images are visually complex, requiring highly trained observers for clinical interpretation. At present, quantitative analysis of ultrasound images is a labour intensive process and the measurements used in practice do not fully exploit the large amount of image data available. This suggests the use of computer aided analysis. The first step in such a system is accurate segmentation.

Segmentation of image data arising from the use of coherent radiation such as ultrasound is complicated by a granular distribution of intensity known as *speckle*. Most algorithms reported in the literature for the purpose of segmentation of ultrasound amplitude or intensity data do not assume an explicit statistical model. To do so would require estimation techniques based on Rayleigh or exponential statistics which are not widely used in image processing. A commonly used method for detecting edges in ultrasound and other forms of coherent imaging is the Laplacian of Gaussian (LoG). Bovik [4] analysed the performance of LoG in detecting edges in speckled images under the assumption of independently distributed intensity data. This is not a good model for ultrasound which tends to be strongly correlated. Bovik found the LoG method tended to produce many false edges and proposed the Ratio of Averages (RoA) method to improve LoG performance. Methods incorporating an explicit statistical model in segmentation of ultrasound include those of Cohen [6] and Ashton and Parker [1]. Cohen modelled both complex and real (bandpass radio-frequency) data using

a Gaussian Markov Random Field. Ashton and Parker acknowledged Rayleigh statistics as a suitable model for the first order statistics of B-mode ultrasound images, but invoked the central limit theorem to justify a Gaussian model for locally averaged images. Other authors have treated speckle as multiplicative noise and used nonlinear methods such as median or mode filters [8] to increase the signal to noise ratio. In this work we investigate the use of a two dimensional AR model. AR models have been successful in modelling image texture in several image processing applications, for example optical aerial images [12]. We apply a two dimensional AR model to complex amplitude data in order to partition the image into regions characterised by distinct second order statistics.

2 Background

In ultrasound imaging a transducer transmits a short acoustic pulse into the medium of interest. The same (or another) transducer then senses the backscattered signal arising from fluctuations in acoustic impedance within the medium. A two dimensional image is constructed by relating the time of arrival to depth and sweeping the beam mechanically or electronically. In ultrasound imaging, as with other forms of coherent imaging, the signal arriving at the transducer may be modelled as the coherent sum of wavelets scattered from sites within the resolution cell. The de-phasing introduced by displacement between randomly positioned scatterers results in speckle. The statistics of laser speckle patterns have been investigated by Goodman [10] while the statistics of speckle in ultrasound have been investigated by Burckhardt [5] and Wagner, Smith, Sandrik and Lopez [13]. The problem of finding the first order statistics for the complex amplitude can be reduced to the classical problem of a random walk in the complex plane. When the amplitude and phase of the kth phasor are statistically independent of each other and of all other phasors, and the phase is uniformly distributed in the interval $[0, 2\pi)$ the probability density function (PDF) for the complex amplitude $x = x_r + j\, x_i$ follows from the central limit theorem [10]

$$p_{r,i}(x_r, x_i) = \frac{1}{2\pi\sigma^2} \exp\left(-\frac{x_r^2 + x_i^2}{2\sigma^2}\right), \tag{1}$$

where the variance σ^2 is determined by the mean square scattering amplitude [10]. Equation 1 is a special case of a complex Gaussian distribution where the real and imaginary components are uncorrelated. This form of the complex Gaussian distribution is termed *circular* Gaussian since contours of constant probability form circles in the complex plane. The assumptions used in deriving Eq. 1 need to be seen in the context of ultrasonic imaging. The assumption of a uniform distribution of phase requires that the average distance between scatterers in the resolution cell be large compared with the wavelength. The number of scatterers must also be large in order to apply the central limit theorem. In practice the latter will only pose a problem when the scatterer density is very low since the limit is reached quite quickly: Wagner et al [13] reported a good approximation to circular Gaussian statistics with approximately 38 scatterers

per cell. The statistics of speckle for a small number of scatterers have been investigated by Jakeman [9].

3 Method

Autoregressive modelling may be defined in terms of linear prediction. For a one dimensional AR sequence, we estimate the signal at a point n as a weighted linear sum of P previous signal values,

$$\hat{x}_n = -a_1^* x_{n-1} - a_2^* x_{n-2}, \ldots, -a_P^* x_{n-P}.$$

Setting $a_0 = 1$ the prediction error is

$$\epsilon_n = x_n - \hat{x}_n = \sum_{j=0}^{P} a_j^* x_{n-j} .$$

The form is similar for a two dimensional signal, however the concept of "past" is replaced by a support region S,

$$\epsilon_{mn} = \sum_{ij \in S} a_{ij}^* x_{(m-i)(n-j)} \tag{2}$$

In this paper we represent an image of size MxN as a vector,

$$\mathbf{x} = [x_j]^T = [x_{00}, ..., x_{0(N-1)}, ..., x_{10}, ..., x_{(M-1)(N-1)}]^T .$$

Hence we define an error image $\boldsymbol{\epsilon}$ as the matrix product

$$\boldsymbol{\epsilon} = \mathbf{A}\mathbf{x} , \tag{3}$$

where $\mathbf{A}$ is a matrix composed of AR parameters. We note that Eq. 3 is approximate as it does not correctly account for data points on the boundary.

3.1 Prediction Error Image

As shown in Section 2 the first order statistics for complex amplitude data may be described by a complex circular Gaussian distribution. We may thus represent an ultrasound image in complex amplitude form by a complex Gaussian random vector. For an image $\mathbf{x}$ of size MxN the PDF has the multivariate form

$$p_x(\mathbf{x}) = \pi^{-MN} |\mathbf{R_x}|^{-1} \exp\left(-\mathbf{x}^{*T} \mathbf{R_x^{-1}} \mathbf{x}\right) . \tag{4}$$

We have assumed zero mean data so that the correlation matrix $\mathbf{R_x}$ is equal to the covariance matrix $\mathbf{C_x}$. Given the transform $\mathbf{A}$, the PDF for the prediction error image is

$$p_\epsilon(\boldsymbol{\epsilon}) = \left(|\mathbf{A}^*||\mathbf{A}|\right)^{-1} p_x(\mathbf{A}^{-1}\boldsymbol{\epsilon})$$

$$= \pi^{-MN} |\mathbf{R}_\epsilon|^{-1} \exp\left(-\boldsymbol{\epsilon}^{*T} \mathbf{R}_\epsilon^{-1} \boldsymbol{\epsilon}\right) , \tag{5}$$

We note that $\mathbf{A}$ is upper diagonal with ones along the diagonal and hence $|\mathbf{A}| = 1$. The correlation matrix for the prediction error image $\mathbf{R}_\epsilon$ is by definition a diagonal matrix with diagonal elements equal to $\mathcal{E}\{\epsilon\,\epsilon^*\} = \sigma_\epsilon^2$, the prediction error variance. The probability density function for the prediction error image is therefore

$$p_\epsilon(\boldsymbol{\epsilon}) = (\sqrt{\pi}\sigma_\epsilon)^{-2MN} \exp\left(- \sum_{j=0}^{MN-1} \frac{|\epsilon_j|^2}{\sigma_\epsilon^2} \right) \tag{6}$$

which is just the PDF for a vector of independent zero mean complex Gaussian random variables.

3.2 Application to Segmentation

Consider an image in which pixels are divided into two classes, for example foreground and background. We may represent this image by two sets L_F and L_B. Given the sets L_F and L_B and representing the image by the data vector $\mathbf{x}$, the likelihood function is

$$p_x(\mathbf{x}|L_F, L_B) = p_{x_F}(\mathbf{x}_F)\, p_{x_B}(\mathbf{x}_B) ,$$

$$= p_{\epsilon_F}(\boldsymbol{\epsilon}_F)\, p_{\epsilon_B}(\boldsymbol{\epsilon}_B) , \tag{7}$$

where $\mathbf{x}_F, \mathbf{x}_B$ represent data in classes F and B. By rewriting Eq. 7 in terms of the prediction error probability density function Eq. 6 we obtain the log likelihood function

$$-N\ln(\pi) - \left[\sum_{j \in L_F} \frac{|\epsilon_{F_j}|^2}{\sigma_{\epsilon_F}^2} + \ln(\sigma_{\epsilon_F}^2) \right] - \left[\sum_{j \in L_B} \frac{|\epsilon_{B_j}|^2}{\sigma_{\epsilon_B}^2} + \ln(\sigma_{\epsilon_B}^2) \right] . \tag{8}$$

We now maximise the image log likelihood given by Eq. 8 (which is the same as maximising the likelihood function itself) by choosing a class for each pixel using the following decision rule:

$$\begin{aligned} &j \in L_B \text{ if } h_F > h_B \\ &j \in L_F \text{ otherwise, where } h_k = \tfrac{|\epsilon_k|^2}{\sigma_{\epsilon_k}^2} + \ln(\sigma_{\epsilon_k}^2) . \end{aligned} \tag{9}$$

Except for the constant $-N\ln(\pi)$ which has no affect on the decision rule, Eq. 8 is the same as that derived for real valued data in [12].

3.3 Implementation

The implementation of the method described above is best thought of in terms of prediction error filtering. For the case of a square quarter plane support region of size 2x2,

$$\begin{bmatrix} \epsilon_{00} \\ \epsilon_{01} \\ \vdots \\ \epsilon_{10} \\ \vdots \\ \epsilon_{(M-2)(N-2)} \end{bmatrix} = \begin{bmatrix} x_{00} & x_{01} & x_{10} & x_{11} \\ x_{01} & x_{02} & x_{11} & x_{12} \\ \vdots & \vdots & \vdots & \vdots \\ x_{10} & \cdots & \cdots & \cdots \\ x_{(M-2)(N-2)} & \cdots & \cdots & \cdots \end{bmatrix} \begin{bmatrix} 1 \\ a_{01} \\ a_{10} \\ a_{11} \end{bmatrix} \tag{10}$$

which may be written compactly as

$$\boldsymbol{\epsilon} = \mathbf{X}\,\mathbf{a}\,. \tag{11}$$

Each row of the data matrix $\mathbf{X}$ is generated by stacking data elements under the support region row-wise. The AR parameter set $\mathbf{a}$ and prediction error variance σ_ϵ^2can be found by solving the Normal equations [11].

$$\frac{1}{MN}\left(\mathbf{X}^{*T}\mathbf{X}\right)\mathbf{a} = \begin{bmatrix} \sigma_\epsilon^2 \\ \mathbf{0} \end{bmatrix}. \tag{12}$$

3.4 Algorithm

1. Select regions F and B representative of foreground class (L_F) and background class (L_B).
2. Compose data matrices $\mathbf{X_F}$ and $\mathbf{X_B}$.
3. Compute AR parameters $\mathbf{a_F}$, $\mathbf{a_B}$ and prediction error variances $\sigma^2_{\epsilon_F}$,$\sigma^2_{\epsilon_B}$.
4. Filter image using $\mathbf{a_F}$ and $\mathbf{a_B}$ to produce prediction error images $\boldsymbol{\epsilon}_F$ and $\boldsymbol{\epsilon}_B$ respectively.
5. Apply the decision rule to estimate a class for each pixel.

4 Results

In order to assess the segmentation method we used a range-theta ($r\,\theta$) ultrasound data set reconstructed to baseband (complex amplitude) format. The radiofrequency (rf) data set is from a 64 element synthetic aperture array (centre frequency 3.3 MHz) applied to a cardiac phantom target [3]. The reconstructed data set is 512 range elements by 102 lateral elements with an axial (range) resolution of 0.35mm per element. An intensity image (Fig. 2a) was generated from the complex data set, gamma corrected with $\gamma = 3.0$. The intensity image was then manually traced by a trained observer to provide the "true" segmentation (Fig. 2b). The manually segmented intensity image is partitioned into foreground and background regions, where we have defined the foreground class

as those pixels arising from the phantom material and the background class as pixels within the phantom cavitys and surrounding the phantom. We next applied the AR/ML algorithm to the complex data set. We used a quarter plane support mask of size 5x5, and estimated the foreground and background model parameters from regions of size 32x32 shown in (Fig. 2b). The AR/ML results are shown in Fig. 2d. For comparison, we generated an edge map using a 21x21 LoG filter with $\sigma = 3.0$. The edge map is shown in Fig. 2c.

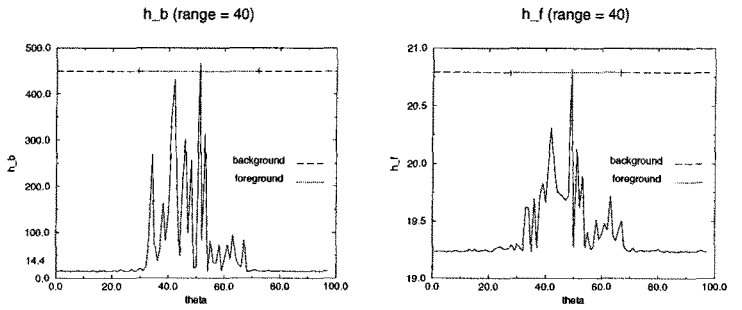

Fig. 1. Decision function plotted for background (left) and foreground models for range = 40 pixels.

5 Discussion and Conclusion

The AR/ML result shown in Fig. 2d produces a reasonably accurate result compared with the manual segmentation shown in Fig. 2b. Using the latter as the "true" hypothesis results in a 10 % Type I error rate (classifying a background pixel as foreground) and a 7.5 % Type II error rate (classifying a foreground pixel as background). The decision function is shown in Fig. 1 for a range of 40 pixels. The graph on the left shows the decision function for the background hypothesis while the graph on the right is the foreground hypothesis. The "true" hypothesis is also indicated on each graph. To interpret these graphs it must be noted that the data values in the background are much less then those in the foreground so that

$$\sigma_B^2 < \sigma_F^2.$$

The graph on the right shows prediction errors (normalised by prediction error variance) that are higher in the foreground class then the background. Although by itself this would not support the true hypothesis, the ML decision is made by comparing the graphs. In this case the decision function follows the true hypothesis quite closely.

We have shown for comparison an edge map produced by the LoG method. Although a direct comparison is difficult we note that the LoG tends to produce

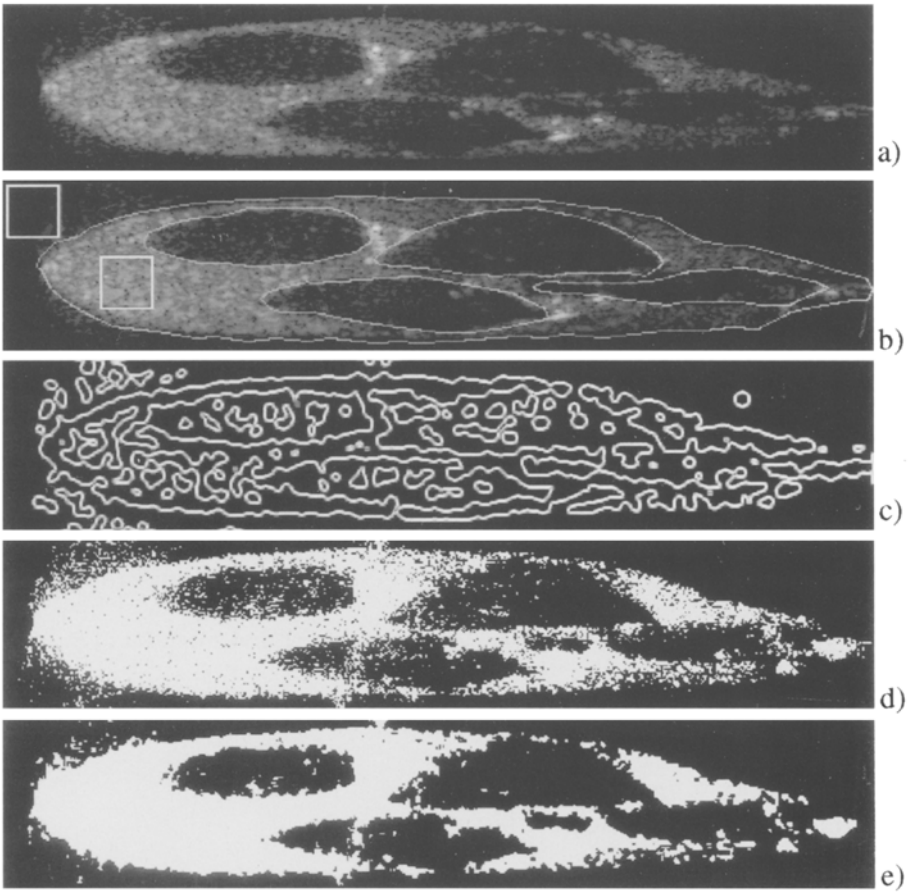

Fig. 2. a) intensity image b) manual segmentation c) LoG, standard deviation 3 pixels d) AR/ML e) AR/ML+median 3x3

many artifacts within the cavity areas. The AR/ML method also classifys incorrectly within the cavity areas but these tend to be isolated pixels. The tendency to produce a "noisy" result is not surprising since no attempt has been made to model spatial correlation in the labelled image. One method of encouraging the formation of regions in the segmented image to use a Bayesian approach with a Markov process describing the region prior [2],[12],[7]. In our case we simply apply a median filter to the segmented image, as shown in Fig. 2e. The median filter is computationally less demanding then the Bayesian techniques and more consistent with the speed of the AR/ML segmentation.

We have used data in range-theta $(r\,\theta)$ form directly, rather then interpolated data. Interpolation does not add to the information present, and may introduce artifacts. The use of $(r\,\theta)$ data does however affect the second order statistics. Since the lateral distance between resolution cells increases with range we expect

the data to become less correlated in the lateral dimension. This effect would be offset partly by the increase in resolution cell size caused by diffraction. One way to counter this effect is to process the $(r\,\theta)$ data in strips of small $\delta\, r$, so that the lateral distance between resolution cells is approximately constant.

In conclusion we have modelled ultrasound data in complex amplitude form as a two dimensional autoregressive random field. Modelled in this way the image likelihood function can be expressed conveniently in terms of prediction error. A maximum likelihood segmentation method for an image consisting of two classes was applied to a cardiac phantom data set. The results show that an autoregressive model captures the second order properties of ultrasound well and that maximum likelihood estimation of regions based on this model produces a segmentation with acceptable Type I and Type II errors.

The authors are grateful to Sriram Krishnan [3] who kindly provided the complex ultrasound data set used in this work.

References

1. E.A. Ashton and K.J. Parker. Multiple resolution bayesian segmentation of ultrasound images. *Ultrasonic Imaging*, 17(4):291–304, October 1995.
2. J. Besag. Spatial interaction and the statistical analysis of lattice systems. *J. Royal Statistical Society B*, B(36):192–225, 1974.
3. Univ. of Michigan Biomedical Ultrasonics Lab. http://bul.eecs.umich.edu/.
4. A.C. Bovik. On detecting edges in speckle imagery. *IEEE Trans. Acoustics, Speech and Signal Processing*, 36(10):1618–1627, October 1988.
5. C.B. Burckhardt. Speckle in ultrasound b-mode scans. *IEEE Trans. Sonics and Ultrasonics*, 25(1), 1978.
6. F.S. Cohen. Modeling of ultrasound speckle with application in flaw detection in metals. *IEEE Trans. Signal Proc.*, 40(3):624–632, March 1992.
7. H. Derin, P.A. Kelly, G. Vezina, and S.G. Labitt. Modeling and segmentation of speckled images using complex data. *IEEE Trans. Geoscience and Remote Sensing*, 28(1):76–87, January 1990.
8. A.N. Evans and M.S. Nixon. Mode filtering to reduce ultrasound speckle for feature extraction. *IEE Proc.-Vis. Image Signal Process,.*, 142(2):87–94, April 1995.
9. E. Jakeman. Speckle statistics with a small number of scatterers. *Optical Engineering*, 23(4):453–461, July/August 1984.
10. J.C.Dainty, editor. *Laser Speckle and Related Phenomena.* Springer-Verlag, New York, 1975.
11. C.W. Therrien. *Discrete Random Signals and Statistical Signal Processing.* Prentice Hall, Englewood Cliffs, NJ 07632, 1992.
12. C.W. Therrien, T.F. Quatieri, and D.E. Dudgeon. Statistical model-based algorithms for image analysis. *Proceedings of IEEE*, 74(4):532–551, April 1986.
13. R.F. Wagner, S.W. Smith, J.M. Sandrik, and H. Lopez. Statistics of speckle in ultrasound b-scans. *IEEE Transactions on Sonics and Ultrasonics*, 30(3):156–163, May 1983.